

SpinDoctor: a Matlab toolbox for diffusion MRI simulation

Jing-Rebecca Li^{a,*}, Van-Dang Nguyen^b, Try Nguyen Tran^a, Jan Valdman^c, Bang Cong Trang^a,
Khieu Van Nguyen^a, Vu Duc Thach Son^a, Hoang An Tran^a, Hoang Trong An Tran^a, Thi Minh
Phuong Nguyen^a

^a*INRIA Saclay, Equipe DEFI, CMAP, Ecole Polytechnique, Route de Saclay, 91128 Palaiseau Cedex, France*

^b*Department of Computational Science and Technology, KTH Royal Institute of Technology, Sweden*

^c*Institute of Mathematics, Faculty of Science, University of South Bohemia, České Budějovice and Institute of Information Theory and Automation of the ASCR, Prague, Czech Republic*

Abstract

The complex transverse water proton magnetization subject to diffusion-encoding magnetic field gradient pulses in a heterogeneous medium can be modeled by the multiple compartment Bloch-Torrey partial differential equation (BTPDE). A mathematical model for the time-dependent apparent diffusion coefficient (ADC), called the H-ADC model, was obtained recently using homogenization techniques on the BTPDE. Under the assumption of negligible water exchange between compartments, the H-ADC model produces the ADC of a diffusion medium from the solution of a diffusion equation (DE) subject to a time-dependent Neumann boundary condition.

This paper describes a publicly available Matlab toolbox called SpinDoctor that can be used 1) to solve the BTPDE to obtain the dMRI signal (the toolbox provides a way of robustly fitting the dMRI signal to obtain the fitted ADC); 2) to solve the DE of the H-ADC model to obtain the ADC; 3) a short-time approximation formula for the ADC is also included in the toolbox for comparison with the simulated ADC. The PDEs are solved by $P1$ finite elements combined with build-in Matlab routines for solving ordinary differential equations. The finite element mesh generation is performed using an external package called Tetgen that is included in the toolbox.

SpinDoctor provides built-in options of including 1) spherical cells with a nucleus; 2) cylindrical cells with a myelin layer; 3) an extra-cellular space (ECS) enclosed either a) in a box or b) in a tight wrapping around the cells; 4) deformation of canonical cells by bending and twisting. 5) permeable membranes for the BT-PDE (the H-ADC assumes negligible permeability). Built-in diffusion-encoding pulse sequences include the Pulsed Gradient Spin Echo and the Oscilating Gradient Spin Echo.

In this paper, we describe how to use the SpinDoctor and illustrate with numerical examples of computing the ADC using the BTPDE, the HADC, and the STA models in spherical cells, cylindrical cells, the myelin layer, and the ECS.

Keywords: Bloch-Torrey equation, diffusion magnetic resonance imaging, finite elements,

*Corresponding author

Email address: jingrebecca.li@inria.fr (Jing-Rebecca Li)

simulation, apparent diffusion coefficient.

1. Introduction

Diffusion magnetic resonance imaging (dMRI) is an imaging modality that can be used to probe the tissue micro-structure by encoding the incoherent motion of water molecules with magnetic field gradient pulses. This motion during the diffusion-encoding time causes a signal attenuation from which the apparent diffusion coefficient (ADC), and possibly higher order diffusion terms, can be calculated [1–3].

For unrestricted diffusion, the root of the mean squared displacement of molecules is given by $\bar{x} = \sqrt{2 \dim \sigma_0 t}$, where \dim is the spatial dimension, σ_0 is the intrinsic diffusion coefficient, and t is the diffusion time. In biological tissue, the diffusion is usually hindered or restricted (for example, by cell membranes) and the mean square displacement is smaller than in the case of unrestricted diffusion. This deviation from unrestricted diffusion can be used to infer information about the tissue micro-structure. The dMRI experimental parameters that can be varied include

1. the diffusion time (one can choose the parameters of the diffusion-encoding sequence, such as Pulsed Gradient Spin Echo (PGSE) [2] and Oscillating Gradient (OGSE) [4]).
2. the magnitude of the diffusion-encoding gradient (when the MRI signal is acquired at low gradient magnitudes, the signal contains only information about the ADC, at higher values, Kurtosis imaging[5] becomes possible);
3. the direction of the diffusion-encoding gradient (many directions may be probed, as in HARDI[6]).

Using dMRI to get tissue structural information in the mammalian brain has been the focus of much experimental and modeling work in recent years [7–14]. The predominant approach up to now has been adding the dMRI signal from simple geometrical components and extracting model parameters of interest. Numerous biophysical models subdivide the tissue into compartments described by spheres, ellipsoids, cylinders, and the extra-cellular space (ECS) [7–9, 11, 12, 15–17]. Some model parameters of interest include axon diameter and orientation, neurite density, dendrite structure, the volume fraction and size distribution of cylinder and sphere components and the effective diffusion coefficient or tensor of the ECS.

Numerical simulations can help deepen the understanding of the relationship between the cellular structure and the dMRI signal and lead to the formulation of appropriate models. They can be also used to investigate the effect of different pulse sequences and tissue features on the measured signal which can be used for the development, testing, and optimization of novel MRI pulse sequences [18, 19].

Two main groups of approaches to the numerical simulation of dMRI are 1) using random walkers to mimic the diffusion process in a geometrical configuration; 2) solving the Bloch-Torrey partial differential equation (BTPDE), which describes the evolution of the complex transverse water proton magnetization under the influence of diffusion-encoding magnetic field gradients pulses.

The first group is referred to as Monte-Carlo simulations in the literature and previous works include [13, 20–23]. A GPU-based acceleration of Monte-Carlo simulation was proposed in [24]. Some software packages using this approach include

1. Camino Diffusion MRI Toolkit developed at UCL (<http://cmic.cs.ucl.ac.uk/camino/>) ;
2. DIFSIM developed at UC San Diego (<http://csci.ucsd.edu/projects/simulation.html>) ;
3. Diffusion Microscopist Simulator[21] developed at Neurospin, CEA .

The second group relies on solving the BTPDE in a geometrical configuration. In [25–27] a simplifying assumption called the narrow pulse approximation was used, where the pulse duration was assumed to be much smaller than the delay between pulses. This assumption allows the solution of the diffusion equation (DE) instead of the more complicated BTPDE. More generally, numerical methods to solve the BTPDE with arbitrary temporal profiles have been proposed in [28–31]. The computational domain is discretized either by a Cartesian grid [28, 29, 32] or finite elements [25–27, 30, 31]. The unstructured mesh of a finite element discretization appeared to be better than a Cartesian grid in both geometry description and signal approximation [30]. For time discretization, both explicit and implicit methods have been used. In [27] a second order implicit time-stepping method called the generalized α -method was used to allow for high frequency energy dissipation. An adaptive explicit Runge-Kutta Chebyshev (RKC) method of second order was used in [29, 30]. It has been theoretically proven that the RKC allows for a much larger time-step compared to the standard explicit Euler method [33]. There is an example showing that the RKC method is faster than the implicit Euler method in [30]. The Crank-Nicolson method (CN) was used in [31] to also allow for second order convergence in time. The efficiency of dMRI simulations is also improved by either a high-performance FEM computing framework [34, 35] for large-scale dMRI simulations on super-computers or a discretization on manifolds for thin-layer and thin-tube media [36].

In this paper, we present a Matlab Toolbox called SpinDoctor that is a simulation pipeline going from the definition of a geometrical configuration through the numerical solution of the BTPDE to the fitting of the ADC from the simulated signal. It also includes two other modules for calculating the ADC. The first is a mathematical model called the H-ADC model, which was obtained recently using homogenization techniques on the BTPDE. In the H-ADC model, the ADC of a geometrical configuration can be computed after solving a diffusion equation (DE) subject to a time-dependent Neumann boundary condition, under the assumption of negligible water exchange between compartments. The second module computes the short time approximation (STA) formula for the ADC. The STA implemented in SpinDoctor includes a recent generalization of this formula to account for finite pulse duration in the PGSE. Both of these two ADC calculations are sensitive to the diffusion-encoding gradient direction, unlike many previous works where the anisotropy of the ADC is neglected in analytical model development. The toolbox is publicly available at:

<https://github.com/jingrebeccali/SpinDoctor>

In summary, SpinDoctor is a Matlab Toolbox that

1. solves the BTPDE in three dimensions to obtain the dMRI signal;
2. robustly fits dMRI signal to obtain the ADC;
3. solves the H-ADC model in three dimensions to obtain the ADC;
4. computes the short-time approximation (STA) of the ADC;
5. computes useful geometrical quantities such as the compartment volumes and surface areas;
6. allows permeable membranes for the BT-PDE (the H-ADC assumes negligible permeability).
7. displays the gradient-direction dependent ADC in 3 dimensions using spherical harmonics interpolation;

SpinDoctor provides the following built-in functionalities:

1. placement of non-overlapping spherical cells (with an optional nucleus) of different radii close to each other;
2. placement of non-overlapping cylindrical cells (with an optional myelin layer) of different radii close to each other in a canonical configuration where they are parallel to the z -axis;
3. inclusion of an extra-cellular space (ECS) that is enclosed either
 - (a) in a tight wrapping around the cells; or
 - (b) in a rectangular box;
4. deformation of the canonical configuration by bending and twisting;

Built-in diffusion-encoding pulse sequences include

1. the Pulsed Gradient Spin Echo (PGSE);
2. the Oscilating Gradient Spin Echo (cos-OGSE, sin-OGSE).

SpinDoctor uses the following methods:

1. it generates a good quality surface triangulation of the user specified geometrical configuration by calling built-in Matlab computational geometry functions;
2. it creates a good quality tetrahedra finite elements mesh from the above surface triangulation by calling Tetgen[37], an external package (executable files are included in the Toolbox package);
3. it constructs finite element matrices for linear finite elements on tetrahedra (P1) using routines from [38];
4. it adds additional degrees of freedom on the compartment interfaces to allow permeability conditions for BTPDE using the formalism in [39];
5. it solves the semi-discretized FEM equations by calling built-in Matlab routines for solving ordinary differential equations (ODEs).

2. Theory

Suppose the user would like to simulate a geometrical configuration of cells with an optional myelin layer or a nucleus. If spins will be leaving the cells or if the user wants to simulate the extra-cellular space (ECS), then the ECS will enclose the geometrical shapes. Let Ω^e be the ECS, Ω_i^{in} the nucleus (or the axon) and Ω_i^{out} the cytoplasm (or the myelin layer) of the i th cell. We denote the interface between Ω_i^{in} and Ω_i^{out} by Γ_i and the interface between Ω_i^{out} and Ω^e by Σ_i , finally the outside boundary of the ECS by Ψ .

2.1. Bloch-Torrey PDE

In diffusion MRI, a time-varying magnetic field gradient is applied to the tissue to encode water diffusion. Denoting the effective time profile of the diffusion-encoding magnetic field gradient by $f(t)$, and let the vector \mathbf{g} contain the amplitude and direction information of the magnetic field

gradient, the complex transverse water proton magnetization in the rotating frame satisfies the Bloch-Torrey PDE:

$$\frac{\partial}{\partial t} M_i^{in}(\mathbf{x}, t) = -I\gamma f(t) \mathbf{g} \cdot \mathbf{x} M_i^{in}(\mathbf{x}, t) + \nabla \cdot (\sigma^{in} \nabla M_i^{in}(\mathbf{x}, t)), \quad \mathbf{x} \in \Omega_i^{in}, \quad (1)$$

$$\frac{\partial}{\partial t} M_i^{out}(\mathbf{x}, t) = -I\gamma f(t) \mathbf{g} \cdot \mathbf{x} M_i^{out}(\mathbf{x}, t) + \nabla \cdot (\sigma^{out} \nabla M_i^{out}(\mathbf{x}, t)), \quad \mathbf{x} \in \Omega_i^{out}, \quad (2)$$

$$\frac{\partial}{\partial t} M^e(\mathbf{x}, t) = -I\gamma f(t) \mathbf{g} \cdot \mathbf{x} M^e(\mathbf{x}, t) + \nabla \cdot (\sigma^e \nabla M^e(\mathbf{x}, t)), \quad \mathbf{x} \in \Omega^e, \quad (3)$$

where $\gamma = 2.67513 \times 10^8 \text{ rad s}^{-1} \text{T}^{-1}$ is the gyromagnetic ratio of the water proton, I is the imaginary unit, σ^l is the intrinsic diffusion coefficient in the compartment Ω_i^l . The magnetization is a function of position \mathbf{x} and time t , and depends on the diffusion gradient vector \mathbf{g} and the time profile $f(t)$. We denote the restriction of the magnetization in Ω_i^{in} by M_i^{in} , and similarly for M_i^{out} and M^e .

Some commonly used time profiles (diffusion-encoding sequences) are:

1. The pulsed-gradient spin echo (PGSE) [2] sequence, with two rectangular pulses of duration δ , separated by a time interval $\Delta - \delta$, for which the profile $f(t)$ is

$$f(t) = \begin{cases} 1, & t_1 \leq t \leq t_1 + \delta, \\ -1, & t_1 + \Delta < t \leq t_1 + \Delta + \delta, \\ 0, & \text{otherwise,} \end{cases} \quad (4)$$

where t_1 is the starting time of the first gradient pulse with $t_1 + \Delta > T_E/2$, T_E is the echo time at which the signal is measured.

2. The oscillating gradient spin echo (OGSE) sequence [4, 40] was introduced to reach short diffusion times. An OGSE sequence usually consists of two oscillating pulses of duration σ , each containing n periods, hence the frequency is $\omega = n \frac{2\pi}{\sigma}$, separated by a time interval $\tau - \sigma$. For a cosine OGSE, the profile $f(t)$ is

$$f(t) = \begin{cases} \cos(n \frac{2\pi}{\sigma} t), & t_1 < t \leq t_1 + \sigma, \\ -\cos(n \frac{2\pi}{\sigma} (t - \tau)), & \tau + t_1 < t \leq t_1 + \tau + \sigma, \\ 0, & \text{otherwise,} \end{cases} \quad (5)$$

where $\tau = T_E/2$.

The BTPDE needs to be supplemented by interface conditions. We recall the interface between Ω_i^{in} and Ω_i^{out} is Γ_i , the interface between Ω_i^{out} and Ω^e is Σ_i , and the outside boundary of the ECS is Ψ . The two interface conditions on Γ_i are the flux continuity and a condition that incorporates a permeability coefficient $\kappa^{in,out}$ across Γ_i :

$$\begin{aligned} \sigma^{in} \nabla M_i^{in}(\mathbf{x}, t) \cdot \mathbf{n}_i^{in} &= -\sigma^{out} \nabla M_i^{out}(\mathbf{x}, t) \cdot \mathbf{n}_i^{out}, & \mathbf{x} \in \Gamma_i, \\ \sigma^{in} \nabla M_i^{in}(\mathbf{x}, t) \cdot \mathbf{n}_i^{in} &= \kappa^{in,out} (M_i^{out}(\mathbf{x}, t) - M_i^{in}(\mathbf{x}, t)), & \mathbf{x} \in \Gamma_i, \end{aligned}$$

where \mathbf{n} is the unit outward pointing normal vector. Similarly, between Ω_i^{out} and Ω^e we have

$$\begin{aligned} \sigma^{out} \nabla M_i^{out}(\mathbf{x}, t) \cdot \mathbf{n}_i^{out} &= -\sigma^e \nabla M^e(\mathbf{x}, t) \cdot \mathbf{n}^e, & \mathbf{x} \in \Sigma_i, \\ \sigma^{out} \nabla M_i^{out}(\mathbf{x}, t) \cdot \mathbf{n}_i^{out} &= \kappa^{out,e} (M^e(\mathbf{x}, t) - M_i^{out}(\mathbf{x}, t)), & \mathbf{x} \in \Sigma_i. \end{aligned}$$

Finally, on the outer boundary of the ECS we have

$$0 = \sigma^e \nabla M^e(\mathbf{x}, t) \cdot \mathbf{n}^e, \quad \mathbf{x} \in \Psi.$$

The BTPDE also needs initial conditions:

$$M_i^{in}(\mathbf{x}, 0) = \rho^{in}, \quad M_i^{out}(\mathbf{x}, 0) = \rho^{out}, \quad M^e(\mathbf{x}, 0) = \rho^e.$$

where ρ is the initial spin density.

The dMRI signal is measured at echo time $t = T_E > \Delta + \delta$ for PGSE and $T_E > 2\sigma$ for OGSE. This signal is the integral of $M(\mathbf{x}, T_E)$:

$$S := \int_{\mathbf{x} \in \cup\{\Omega_i^{in}, \Omega_i^{out}, \Omega^e\}} M(\mathbf{x}, T_E) d\mathbf{x}. \quad (6)$$

In a dMRI experiment, the pulse sequence (time profile $f(t)$) is usually fixed, while \mathbf{g} is varied in amplitude (and possibly also in direction). When \mathbf{g} varies only in amplitude (while staying in the same direction), S is plotted against a quantity called the b -value. The b -value depends on \mathbf{g} and $f(t)$ and is defined as

$$b(\mathbf{g}) = \gamma^2 \|\mathbf{g}\|^2 \int_0^{T_E} du \left(\int_0^u f(s) ds \right)^2.$$

For PGSE, the b -value is [2]:

$$b(\mathbf{g}, \delta, \Delta) = \gamma^2 \|\mathbf{g}\|^2 \delta^2 (\Delta - \delta/3). \quad (7)$$

For the cosine OGSE with *integer* number of periods n in each of the two durations σ , the corresponding b -value is [28]:

$$b(\mathbf{g}, \sigma) = \gamma^2 \|\mathbf{g}\|^2 \frac{\sigma^3}{4n^2\pi^2} = \gamma^2 \|\mathbf{g}\|^2 \frac{\sigma}{\omega^2}. \quad (8)$$

The reason for these definitions is that in a homogeneous medium, the signal attenuation is $e^{-\sigma b}$, where σ is the intrinsic diffusion coefficient.

2.2. Fitting the ADC from the dMRI signal

An important quantity that can be derived from the dMRI signal is the ‘‘Apparent Diffusion Coefficient’’ (ADC), which gives an indication of the root mean squared distance travelled by water molecules in the gradient direction $\mathbf{g}/\|\mathbf{g}\|$, averaged over all starting positions:

$$ADC := -\frac{\partial}{\partial b} \log \frac{S(b)}{S(0)} \Big|_{b=0}. \quad (9)$$

We numerically compute ADC by a polynomial fit of

$$\log S(b) = c_0 + c_1 b + \dots + c_n b^n,$$

increasing n from 1 onwards until we get the value of c_1 to be stable within a numerical tolerance.

2.3. H-ADC model

In a previous work [41], a PDE model for the time-dependent ADC was obtained starting from the Bloch-Torrey equation, using homogenization techniques. In the case of negligible water exchange between compartments (low permeability), there is no coupling between the compartments, at least to the quadratic order in \mathbf{g} , which is the ADC term. The ADC in compartment Ω is given by

$$HADC = \sigma - \frac{1}{\int_0^{TE} F(t)^2 dt} \int_0^{TE} F(t) h(t) dt, \quad (10)$$

where

$$h(t) = \frac{1}{|\Omega|} \int_{\partial\Omega} \omega(\mathbf{x}, t) (\mathbf{u}_{\mathbf{g}} \cdot \mathbf{n}) ds \quad (11)$$

is a quantity related to the directional gradient of a function ω that is the solution of the homogeneous diffusion equation (DE) with Neumann boundary condition and zero initial condition:

$$\begin{aligned} \frac{\partial}{\partial t} \omega(\mathbf{x}, t) - \nabla (\sigma \nabla \omega(\mathbf{x}, t)) &= 0, & \mathbf{x} \in \Omega, \\ \sigma \nabla \omega(\mathbf{x}, t) \cdot \mathbf{n} &= \sigma F(t) \mathbf{u}_{\mathbf{g}} \cdot \mathbf{n}, & \mathbf{x} \in \partial\Omega, \\ \omega(\mathbf{x}, 0) &= 0, & \mathbf{x} \in \Omega, \end{aligned} \quad (12)$$

\mathbf{n} being the outward normal and $t \in [0, TE]$. The above set of equations, (10)-(12), comprise the homogenized model that we call the H-ADC model.

2.4. Short diffusion time approximation of the ADC

A well-known formula for the ADC in the short diffusion time regime is the following short time approximation (STA) [42, 43]:

$$STA = \sigma \left(1 - \frac{4\sqrt{\sigma}}{3\sqrt{\pi}} \sqrt{\Delta} \frac{A}{\dim V} \right),$$

where $\frac{A}{V}$ is the surface to volume ratio and σ is the intrinsic diffusivity coefficient. In the above formula the pulse duration δ is assumed to be very small compared to Δ . A recent correction to the above formula [41], taking into account the finite pulse duration δ and the gradient direction $\mathbf{u}_{\mathbf{g}}$, is the following:

$$STA = \sigma \left[1 - \frac{4\sqrt{\sigma}}{3\sqrt{\pi}} C_{\delta, \Delta} \frac{A_{\mathbf{u}_{\mathbf{g}}}}{V} \right], \quad (13)$$

where

$$A_{\mathbf{u}_{\mathbf{g}}} = \int_{\partial\Omega} (\mathbf{u}_{\mathbf{g}} \cdot \mathbf{n})^2 ds,$$

and

$$C_{\delta, \Delta} = \frac{4}{35} \frac{(\Delta + \delta)^{7/2} + (\Delta - \delta)^{7/2} - 2(\delta^{7/2} + \Delta^{7/2})}{\delta^2 (\Delta - \delta/3)} = \sqrt{\Delta} \left(1 + \frac{1}{3} \frac{\delta}{\Delta} - \frac{8}{35} \left(\frac{\delta}{\Delta} \right)^{3/2} + \dots \right).$$

When $\delta \ll \Delta$, the value $C_{\delta, \Delta}$ is approximately $\sqrt{\Delta}$.

3. Method

Below is a chart describing the work flow of SpinDoctor.

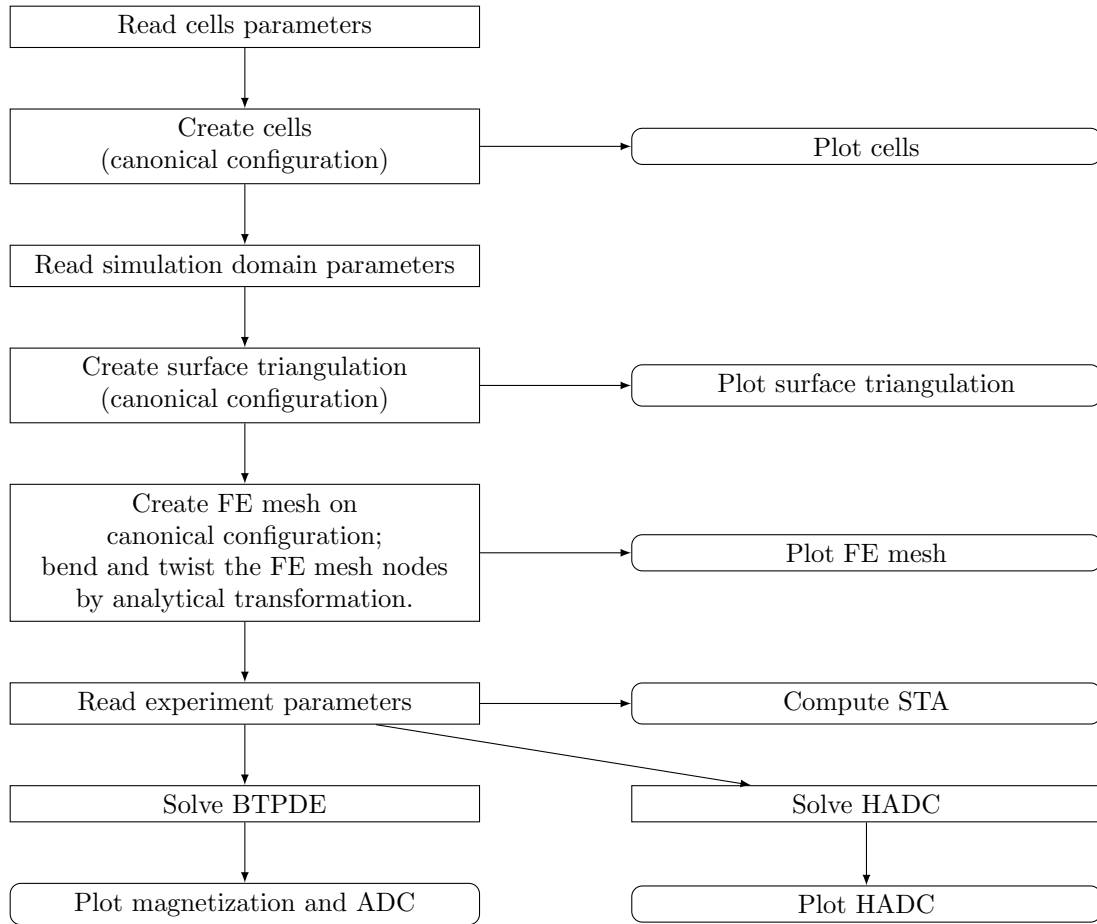


Figure 1: Flow chart describing the work flow of SpinDoctor

The physical units of the quantities in the input files for SpinDoctor are shown in Table 1, in particular, the length is in μm and the time is in μs .

Parameter	Unit
length	μm
time	μs
diffusion coefficient	$\mu\text{m}^2/\mu\text{s} = \text{mm}^2/\text{s}$
permeability coefficient	$\mu\text{m}/\mu\text{s} = \text{m}/\text{s}$
b-value	$\mu\text{s}/\mu\text{m}^2 = \text{s}/\text{mm}^2$
q-value	$(\mu\text{s}\mu\text{m})^{-1}$

Table 1: Physical units of the quantities in the input files for SpinDoctor.

Below we discuss the various components of SpinDoctor in more detail.

3.1. Read cells parameters

The user provides an input file for the cell parameters, in the format described in Table 2.

Line	Variable name	Example	Explanation
1	cell_shape	1	1 = spheres; 2 = cylinders;
2	fname_params_cells	'current_cells'	file name to store cells description
3	ncell	10	number of cells
4	Rmin	1.5	min Radius
5	Rmax	2.5	max Radius
6	dmin	1.5	min (%) distance between cells: $dmin \times \frac{(Rmin+Rmax)}{2}$
7	dmax	2.5	max (%) distance between cells $dmax \times \frac{(Rmin+Rmax)}{2}$
8	para_deform	0.05 0.05	$[\alpha \ \beta]$; α defines the amount of bend; β defines the amount of twist
9	Hcyl	20	height of cylinders

Table 2: Input file containing cells parameters.

3.2. Create cells (canonical configuration)

SpinDoctor supports the placement of a group of non-overlapping cells in close vicinity to each other. There are two proposed configurations, one composed of spheres, the other composed of cylinders. The algorithm is described in Algorithm 1.

3.3. Plot cells

SpinDoctor provides a routine to plot the cells to see if the configuration is acceptable (see Fig. 2).

Algorithm 1: Placing n_{cell} non-overlapping cells.

Generate a large number of possible cell centers.

Compute the distance, $dist$, between the current center and previously accepted cells.

Find the intersection of $[dist - d_{max} \times R_{mean}, dist - d_{min} \times R_{mean}]$ and $[R_{min}, R_{max}]$, where $R_{mean} = \frac{R_{min} + R_{max}}{2}$. If the intersection is not empty, then take the middle of the intersection as the new radius and accept the new center. Otherwise, reject the center.

Loop through the possible centers until get n_{cell} accepted cells.

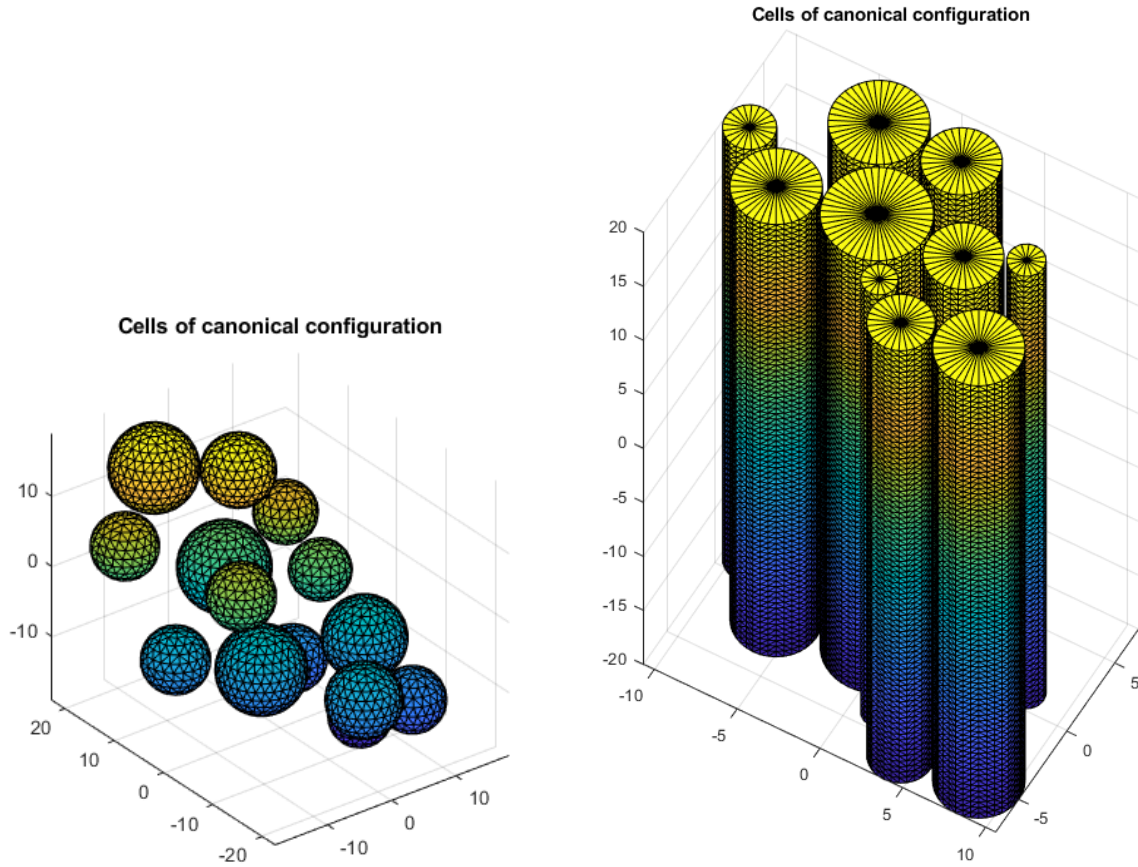


Figure 2: SpinDoctor plots cells in the canonical configuration.

3.4. Read simulation domain parameters

The user provides an input file for the simulation domain parameters, in the format described in Table 3.

Line	Variable name	Example	Explanation
1	Rratio	0.0	if Rratio is outside [0,1], it is set to 0; else $Rratio = \frac{R_{in}}{R_{out}}$;
2	include_ECS	2	0 = no ECS; 1 = box ECS; 2 = tight wrap ECS;
3	ECS_gap	0.3	ECS thickness: a. if box: as percentage of domain length; b. if tight wrap: as percentage of mean radius
4	dcoeff_IN	0.002	diffusion coefficient in IN cmpt: a. nucleus; b. axon (if there is myelin);
5	dcoeff_OUT	0.002	diffusion coefficient in OUT cmpt: a. cytoplasm; b. axon (if there is no myelin);
6	dcoeff_ECS	0.002	diffusion coefficient in ECS cmpt;
7	ic_IN	1	initial spin density in In cmpt: a. nucleus; b. axon (if there is myelin)
8	ic_OUT	1	initial spin density in OUT cmpt: a. cytoplasm; b. axon (if there is no myelin);
9	ic_ECS	1	initial spin density in ECS cmpt:
10	kappa_IN_OUT	1e-5	permeability between IN and OUT cmpts: a. between nucleus and cytoplasm; b. between axon and myelin;
11	kappa_OUT_ECS	1e-5	permeability between OUT and ECS cmpts: a. if no nucleus: between cytoplasm and ECS; b. if no myelin: between axon and ECS;
12	Htetgen	-1	Requested tetgen mesh size; -1 = Use tetgen default;
13	tetgen_cmd	'SRC/TETGEN/ tetGen/win64/ tetgen'	path to tetgen_cmd

Table 3: Input file of simulation domain parameters.

3.5. Create surface triangulation

Finite element mesh generation software requires a good surface triangulation. This means the surface triangulation needs to be water-tight and does not self-intersect. How closely these requirements are met in floating point arithmetic has a direct impact on the quality of the finite element mesh generated.

It is often difficult to produce a good surface triangulation for arbitrary geometries. Thus, we restrict the allowed shapes to cylinders and spheres. Below in Algorithms 2 and 3 we describe how

to obtain a surface triangulation for spherical cells with nucleus, cylindrical cells with myelin layer, and the ECS (box or tightly wrapped). We describe a canonical configuration where the cylinders are placed parallel to the z -axis. More general shapes are obtained from the canonical configuration by coordinate transformation in a later step.

Algorithm 2: Surface triangulation of spherical cells and ECS.

Suppose we have n_{cell} spherical cells with nucleus. Denote a sphere with center c and radius R by $S(c, R)$, we use the built-in functions (convex hull, delaunay triangulation) in Matlab to get its surface triangulation, $T(c, R)$. Call the radii of the nucleus $r_1, \dots, r_{n_{cell}}$ and the radii of the cells $R_1, \dots, R_{n_{cell}}$. Then the boundaries between the cytoplasm and the nucleus are

$$\{\Gamma_i = T(c_i, r_i)\}, i = 1, \dots, n_{cell};$$

and between the cytoplasm and the ECS

$$\{\Sigma_i = T(c_i, R_i)\}, i = 1, \dots, n_{cell};$$

For the box ECS, we find the coordinate limits of the set

$$\bigcup_i S(c_i, R_i) \in [x_0, x_f] \times [y_0, y_f] \times [z_0, z_f]$$

and add a gap $k = \text{ECS_gap} \times \max\{x_f - x_0, y_f - y_0, z_f - z_0\}$ to make a box

$$B = [x_0 + k, x_f + k] \times [y_0 - k, y_f + k] \times [z_0 - k, z_f + k].$$

We put 2 triangles on each face of B to make a surface triangulation Ψ with 12 triangles. For the tight-wrap ECS, we increase the cell radius by a gap size and take the union

$$W = \bigcup_i S(c_i, R_i + (\text{ECS_gap} \times R_{mean})),$$

where $R_{mean} = \frac{(R_{min} + R_{max})}{2}$. We use the alphaShape function in Matlab to find a surface triangulation Ψ that contains W .

Algorithm 3: Surface triangulation of cylindrical cells and ECS.

Suppose we have n_{cell} cylindrical cells with a myelin layer, all with height H . Denote a disk with center c and radius R by $D(c, R)$, and the circle with the same center and radius by $C(c, R)$. Let the radii of the axons be $r_1, \dots, r_{n_{cell}}$ and the radii of the cells be $R_1, \dots, R_{n_{cell}}$, meaning the thickness of the myelin layer is $R_i - r_i$. The boundary between the axon and the myelin layer is:

$$C(c_i, r_i) \times [-H/2, H/2]$$

We discretize $C(c_i, r_i)$ as a polygon $P(c_i, r_i)$ and place one at $z = -H/2$ and one at $z = H/2$. Then we connect the corresponding vertices of $P(c_i, r_i) \times \{-H/2\}$ and $P(c_i, r_i) \times \{H/2\}$ and add a diagonal on each panel to get a surface triangulation Γ_i . Between the myelin layer and the ECS we discretize $C(c_i, R_i)$ as a polygon and place one at $z = -H/2$ and one at $z = H/2$ to get a surface triangulation Σ_i . For the box ECS, we find the coordinate limits of the union of $D(c_i, R_i)$ and add a gap to make a rectangle in two dimensions. Then we place the rectangle at $z = -H/2$ and at $z = H/2$ to get a box. Finally, the box is given a surface triangulation with 12 triangles. For tight-wrap ECS, we increase the cell radius by a gap size and take the union

$$W = \bigcup_i D(c_i, R_i + kR_{mean}).$$

We use the alphaShape function in Matlab to find a two dimensional polygon Q that contains W . We place Q at $z = -H/2$ and at $z = H/2$ and connect corresponding vertices, adding a diagonal on each panel. Suppose Q is a polygon with n vertices, then the surface triangulation of the side of the ECS will have $2n$ triangles.

The above procedure produces a surface triangulation for the boundaries that are parallel to z -axis. We now must close the top and bottom. The top and bottom boundaries is just the interior of Q . However, the surface triangulation cannot be done on Q directly. We must cut out $D(c_i, R_i)$, the disk which touches the axon, and $A_i = D(c_i, R_i) - D(c_i, r_i)$, the annulus which touches the myelin. Then we triangulate $Q - \bigcup_i D_i - \bigcup_i A_i$ using the Matlab built-in function that triangulates a polygon with holes to get the boundary that touches the ECS. The surface triangulation for A_i and $D(c_i, R_i)$ are straightforward.

3.6. Plot surface triangulation

SpinDoctor provides a routine to plot the surface triangulation (see Fig. 3).

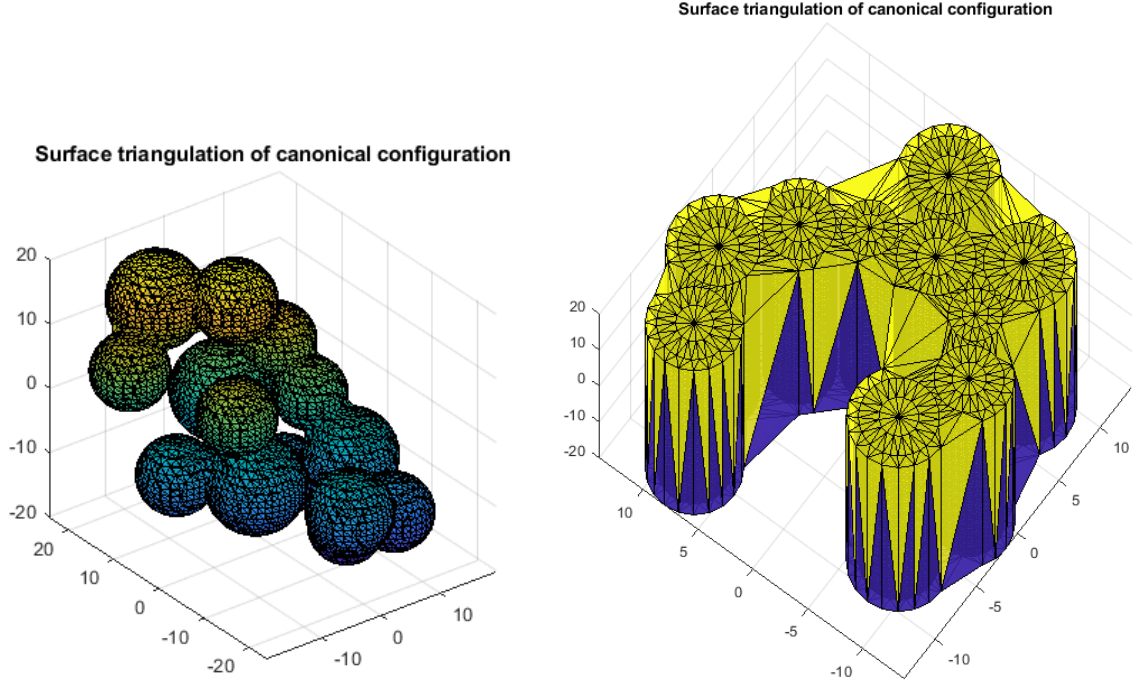


Figure 3: SpinDoctor plots the surface triangulation of the canonical configuration. Left: sphere cells with ECS; Right: cylindrical cells, myelin layer, and ECS.

3.7. Finite element mesh generation

SpinDoctor calls Tetgen[37], an external package (executable files are included in the toolbox package), to create a tetrahedra finite elements mesh from the surface triangulation generated by Algorithms 2 and 3. The FE mesh is generated on the canonical configuration. The numbering of the compartments and boundaries used by SpinDoctor are given in Tables 4 and 5. The labels are related to the values of the intrinsic diffusion coefficient, the initial spin density, and the permeability requested by the user. Then the FE mesh nodes are deformed analytically by a coordinate transformation, described in Algorithm 4.

Spherical cells without nucleus			
Cmpt	Cytoplasm	Nucleus	ECS
Label	OUT		ECS
Number	$[1 : n_{cell}]$		$n_{cell} + 1$
Spherical cells with nucleus			
Cmpt	Cytoplasm	Nucleus	ECS
Label	OUT	IN	ECS
Number	$[1 : n_{cell}]$	$[n_{cell} + 1 : 2n_{cell}]$	$2n_{cell} + 1$
Cylindrical cells without myelin			
Cmpt	Axon	Myelin	ECS
Label	OUT		ECS
Number	$[1 : n_{cell}]$		$n_{cell} + 1$
Cylindrical cells with myelin			
Cmpt	Axon	Myelin	ECS
Label	IN	OUT	ECS
Number	$[1 : n_{cell}]$	$[n_{cell} + 1 : 2n_{cell}]$	$2n_{cell} + 1$

Table 4: The labels and numbers of compartments.

Spherical cells without nucleus			
Boundary	Sphere		Outer ECS boundary
Label	OUT_ECS		$\kappa = 0$
Number	$1 : n_{cell}$		$n_{cell} + 1$
Spherical cells with nucleus			
Boundary	Outer sphere	Inner sphere	Outer ECS boundary
Label	OUT_ECS	IN_OUT	$\kappa = 0$
Number	$1 : n_{cell}$	$n_{cell} + 1 : 2n_{cell}$	$2n_{cell} + 1$
Cylindrical cells without myelin			
Boundary	Cylinder side wall	Cylinder top and bottom	Outer ECS boundary minus cylinder top/bottom
Label	OUT_ECS	$\kappa = 0$	$\kappa = 0$
Number	$2[1 : n_{cell}] - 1$	$2[1 : n_{cell}]$	$2n_{cell} + 1$
Cylindrical cells with myelin			
Boundary	Inner cylinder side wall	Inner cylinder top and bottom	
Label	IN_OUT	$\kappa = 0$	
Number	$4[1 : n_{cell}] - 3$	$4[1 : n_{cell}] - 2$	
Boundary	Outer cylinder side wall	Outer cylinder top and bottom	Outer ECS boundary minus cylinder top/bottom
Label	OUT_ECS	$\kappa = 0$	$\kappa = 0$
Number	$4[1 : n_{cell}] - 1$	$4[1 : n_{cell}]$	$4n_{cell} + 1$

Table 5: The labels and numbers of boundaries.

Algorithm 4: Bending and twisting of the FE mesh of the canonical configuration.

The external package Tetgen[37] generates the finite element mesh that keeps track of the different compartments and the interfaces between them. The mesh is saved in several text files.

The connectivity matrices of the finite elements and facets are not modified by the coordinates transformation described below. The nodes are transformed by bending and twisting as described next.

The set of FE mesh nodes $\{x_i, y_i, z_i\}$ are transformed in the following way. Define the rotation matrix taking the vector v_1 to v_2 by $R(v_1, v_2)$. Twisting around the z -axis with a user-chosen twisting parameter α_{twist} is defined by

$$\begin{bmatrix} x \\ y \\ z \end{bmatrix} \rightarrow \begin{bmatrix} R \left(\begin{bmatrix} 1 \\ 0 \end{bmatrix}, \begin{bmatrix} \cos(\alpha_{twist}z) \\ \sin(\alpha_{twist}z) \end{bmatrix} \right) \begin{bmatrix} x \\ y \end{bmatrix} \\ z \end{bmatrix};$$

Bending on the $x - z$ plane with a user-chosen bending parameter α_{bend} is defined by

$$\begin{bmatrix} x \\ y \\ z \end{bmatrix} \rightarrow \begin{bmatrix} x + \alpha_{bend}z^2 \\ y \\ z \end{bmatrix};$$

Given $[\alpha_{bend}, \alpha_{twist}]$, bending is performed after twisting.

3.8. Plot FE mesh

SpinDoctor provides a routine to plot the FE mesh (see Fig. 4 for cylinders and ECS that have been bent and twisted).

FE Mesh Inner cmpts: 1 2 3 4 5 6 7 8 9 10

FE Mesh ECS cmpt: 11

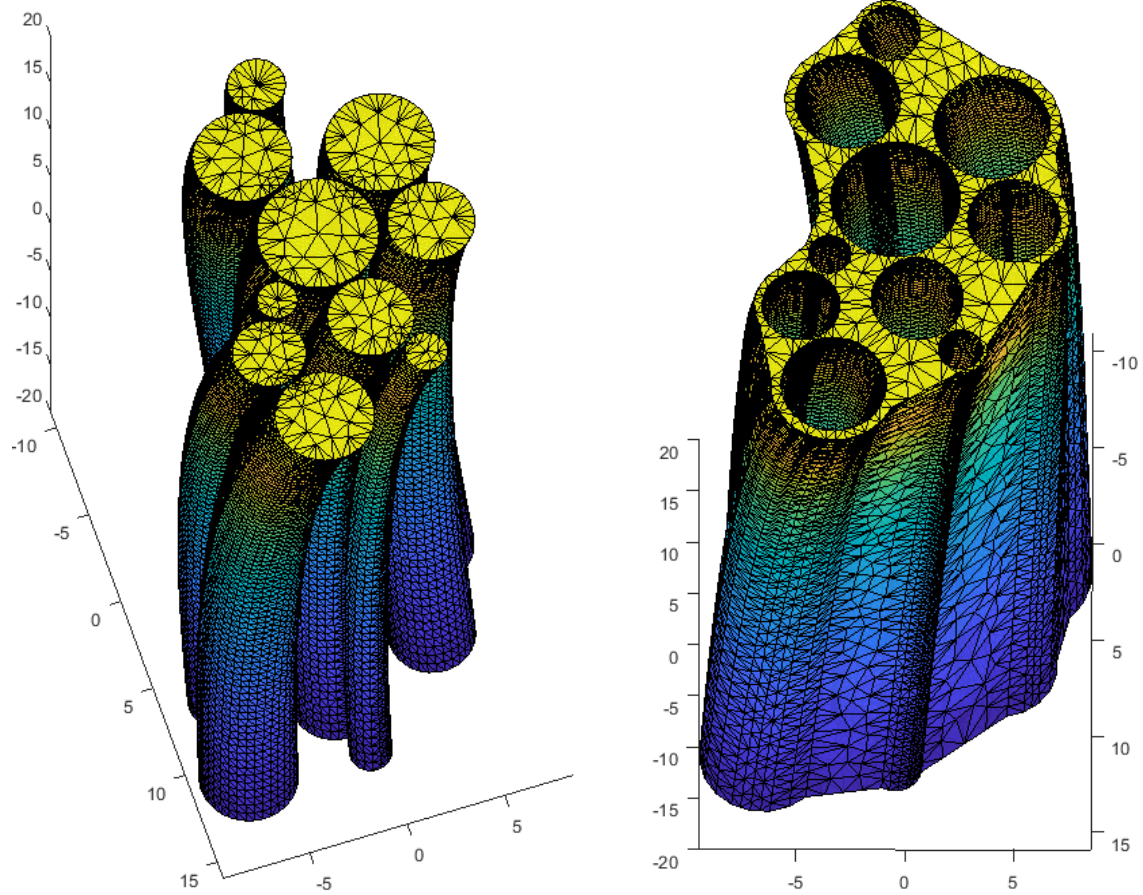


Figure 4: FE mesh of cylinders and ECS after bending and twisting. Compartment number is 1 to 10 for the cylinders and 11 for the ECS.

3.9. Read experimental parameters

The user provides an input file for the simulation experimental parameters, in the format described in Table 6.

Line	Variable name	Example	Explanation
1	ngdir	20	number of gradient direction; if $ngdir > 1$, the gradient directions are distributed uniformly on a sphere; if $ngdir = 1$, take the gradient direction from the line below;
2	gdir	1.0 0.0 0.0	gradient direction; No need to normalize;
3	nexperi	3	number of experiments;
4	sdeltavec	2500 10000 10000	small delta;
5	bdeltavec	2500 10000 10000	big delta;
6	seqvec	1 2 3	diffusion sequence of experiment; 1 = PGSE; 2 = OGSEsin; 3 = OGSEcos;
7	npervec	0 10 10	number of period of OGSE;
8	solve_hadc	1	0 = do not solve HADC; Otherwise solve HADC;
9	rtol_deff, atol_deff	1e-4 1e-4	$[r_{tol} \ a_{tol}]$; relative and absolute tolerance for HADC ODE solver;
10	solve_btpde	1	0: solve BTPDE; Otherwise do not solve BTPDE;
11	rtol_bt, atol_bt	1e-5 1e-5	$[r_{tol} \ a_{tol}]$; relative and absolute tolerance for BTPDE ODE solver;
12	nb	2	number of b-values;
13	blimit	0	0=specify bvec; 1=specify[bmin,bmax]; 2 = specify[gmin,gmax];
14	const_q	0	0: use input bvalues for all experiments; 1: take input bvalues for the first experiment and use the same q for the remaining experiments
15	bvalues	0 50 100 200	bvalues or [bmin, bmax] or [gmin, gmax]; depending on line 13;

Table 6: Input file for simulation experiment parameters.

3.10. BTPDE

The spatial discretization of the BTPDE is based on a finite element method where *interface (ghost) elements* [30] are used to impose the permeable interface conditions. The time stepping is done

using the Matlab built-in ODE routine ode23t. See Algorithm 5.

Algorithm 5: BTPDE.

FE matrices are generated for each compartment by the finite element method with continuous piecewise linear basis functions (known as P_1). The basis functions are denoted as φ_k for $k = 1, \dots, N_v$, where N_v denotes the number of mesh nodes (vertices). All matrices are sparse matrices. \mathbf{M} and \mathbf{S} are known in the FEM literature as mass and stiffness matrices which are defined as follows:

$$\mathbf{M}_{ij} = \int_{\Omega} \varphi_i \varphi_j d\mathbf{x}, \quad \mathbf{S}_{ij} = \int_{\Omega} \sigma_i \nabla \varphi_i \cdot \nabla \varphi_j d\mathbf{x}.$$

\mathbf{J} has a similar form with the mass matrix but it is scaled with the coefficient $\mathbf{g} \cdot \mathbf{x}$, we therefore call it the scaled-mass matrix

$$\mathbf{J}_{ij} = \int_{\Omega} \mathbf{g} \cdot \mathbf{x} \varphi_i \varphi_j d\mathbf{x}.$$

We construct the matrix based on the flux matrix \mathbf{Q}

$$\mathbf{Q}_{ij} = \int_{\partial\Omega} w \varphi_i \varphi_j ds$$

where a scalar function w is used as an interface marker. The matrices are assembled from local element matrices and the assembly process is based on vectorized routines of [38], which replace expensive loops over elements by operations with 3-dimensional arrays. All local element matrices in the assembly of \mathbf{S} , \mathbf{M} , \mathbf{J} are evaluated at once and stored in a full matrix of size $4 \times 4 \times N_e$, where N_e denotes the number of tetrahedral elements. The assembly of \mathbf{Q} is even simpler; all local matrices are stored in a full matrix of size $3 \times 3 \times n_{be}$, where n_{be} denotes the number of boundary triangles.

Double nodes are placed at the interfaces between compartments connected by permeable membrane. $\overline{\mathbf{Q}}$ is used to impose the interface conditions and it is associated with the *interface (ghost) elements*. Specifically, assume that the double nodes are defined in a pair of indices $\{i, \bar{i}\}$, $\overline{\mathbf{Q}}$ is defined as the following

$$\overline{\mathbf{Q}}_{ij} = \begin{cases} \mathbf{Q}_{ij}, & \text{if vertex } i \text{ and } j \text{ belong to one interface} \\ -\mathbf{Q}_{\bar{i}\bar{j}} & \text{if vertex } i \text{ and } j \text{ belong to two different interfaces} \end{cases}$$

The fully coupled linear system has the following form

$$\mathbf{M} \frac{\partial \xi}{\partial t} = - \left(I \gamma f(t) \mathbf{J} + \mathbf{S} + \overline{\mathbf{Q}} \right) \xi \quad (14)$$

where ξ is the approximation of the magnetization M . SpinDoctor calls Matlab built-in ODE routine ode23t to solve the semi-discretized equation.

3.11. H-ADC model

Similarly, the DE of the H-ADC model is discretized by finite elements. See Algorithm 6.

<p>Algorithm 6: HADC model.</p> <p>Eq. (12) can be discretized similarly as described for the BTPDE and has the matrix form</p> $\mathbf{M} \frac{\partial \zeta}{\partial t} = -\mathbf{S} \zeta + \mathbf{Q} \bar{\zeta} \quad (15)$ <p>where ζ is the approximation of w and $\bar{\zeta}_i = \sigma_i F(t) \mathbf{u}_g \cdot \mathbf{n}(\mathbf{x}_i)$. We note that the matrices here are assembled and solve separately for each compartment. SpinDoctor calls Matlab built-in ODE routine ode23t to solve the semi-discretized equation.</p>
--

3.12. Some important output quantities

In Table 7 we list some useful quantities that are the outputs of SpinDoctor. The braces in the "Size" column denote Matlab cell data structure and the brackets denote Matlab matrix data structure.

Variable name	Size	Explanation
TOUT	{nexperi × nb × Ncmpt}[1 × nt]	ODE time discretization
YOUT	{nexperi × nb × Ncmpt}[Nnodes × nt]	Magnetization
MF_cmpts	[Ncmpt × nexperi × nb]	integral of magnetization at TE in each compartment.
MF_allcmpts	[nexperi × nb]	integral of magnetization at TE summed over all compartments.
ADC_cmpts	[Ncmpt × nexperi]	ADC in each compartment.
ADC_allcmpts	[nexperi × 1]	ADC summed over all compartments.
ADC_cmpts_dir	[ngdir × Ncmpt × nexperi]	ADC in each compartment in each direction.
ADC_allcmpts_dir	[ngdir × nexperi × 1]	ADC summed over all compartments in each direction.

Table 7: Some important SpinDoctor output quantities.

4. Numerical results

4.1. Comparison with reference solution

First we compare the results from SpinDoctor with the reference solution using the Matrix Formalism method [44] for a variety of b -values and permeability coefficients. Plotted in Fig. 5 are the dMRI signals using the BTPDE solve in SpinDoctor and the Matrix Formalism method. The maximum relative errors between SpinDoctor and the reference signal are 2.26%, 1.06%, and 0.68% for the three permeability coefficients simulated.

4.2. Comparison of BTPDE and HADC with Short Time Approximation

In Fig. 6 we show that both BTPDE and HADC solutions match the STA values at short diffusion times for cylindrical cells (compartments 1 to 5). We also show that for the ECS (compartment 6), the STA is too low, because it does not account for the fact that spins in the ECS can diffuse around several cylinders. This also shows that when the interfaces are impermeable, the BTPDE ADC and that from the H-ADC model are identical. The diffusion-encoding sequence here is cosine OGSE with 6 periods.

4.3. Permeable membranes

In Fig. 7 we show the effect of permeability: the BTPDE model includes permeable membranes ($\kappa = 1 \times 10^{-3}$ m/s) whereas the H-ADC has impermeable membranes. We see in the permeable case, the ADC in the spheres are higher than in the impermeable case, whereas the ECS show reduced ADC because the faster diffusing spins in the ECS are allowed to move into the slowly diffusion spherical cells. We note that in the permeable case, the ADC in each compartment is obtained by using the fitting formula involving the logarithm of the dMRI signal, and we defined the "signal" in a compartment as the total magnetization in that compartment at TE, which is just the integral of the solution of the BTPDE in that compartment.

4.4. Myelin layer

In Fig. 8 we show the diffusion in cylindrical cells, the myelin layer, and the ECS. The ADC is higher in the myelin layer than in the cells, because for spins in the myelin layer diffusion occurs in the tangential direction (around the circle). At longer diffusion times, the ADC of both the myelin layer and the cells becomes very low. The ADC is the highest in the ECS, because the diffusion distance can be longer than the diameter of a cell, since the diffusing spins can move around multiple cells.

4.5. Twisting and bending

In Fig. 9 we show the effect of bending and twisting in cylindrical cells in multiple gradient directions. The HADC is obtained in 20 directions uniformly distributed in the sphere. We used spherical harmonics interpolation to interpolate the HADC in the entire sphere. Then we deformed the radius the unit sphere to be proportional to the interpolated HADC and plotted the 3D shape. The color axis also indicates the value of the interpolated HADC.

4.6. Timing

In Table 8 we give the average computational times for solving the BTPDE and the HADC. All simulations were performed on Intel(R) Core(TM) i5-4210U CPU @ 1.70 GHz 2.40 GHz, running Windows 10 (1809). The geometrical configuration includes 2 axons and a tight wrap ECS, the simulated sequence is PGSE ($\delta = 2.5$ ms, $\Delta = 5$ ms). In the impermeable case, the compartments are uncoupled, and the computational times are given separately for each compartment. In the permeable membrane case, the compartments are coupled, and the computational time is for the coupled system (relevant to the BTPDE only).

	FE mesh size	BTPDE $b = 50 \text{ s/mm}^2$	BTPDE $b = 1000 \text{ s/mm}^2$	HADC
Uncoupled: Axons	5865 nodes, 19087 ele	7.89 sec	9.07 sec	8.80 sec
Uncoupled: ECS	6339 nodes, 19618 ele	10.14 sec	13.95 sec	11.87 sec
Coupled: Axons+ECS	7344 nodes, 38705 ele	39.14 sec	43.24 sec	N/A

Table 8: Computational times for solving the BTPDE and the HADC. All simulations were performed on Intel(R) Core(TM) i5-4210U CPU @ 1.70 GHz 2.40 GHz, running Windows 10 (1809). The geometrical configuration includes 2 axons and a tight wrap ECS, the simulated sequence is PGSE ($\delta = 2.5\text{ms}$, $\Delta = 5\text{ms}$).

5. Discussion

Built upon Matlab, SpinDoctor is a software package that seeks to reduce the work required to perform numerical simulations for dMRI for prototyping purposes. There have been software packages for dMRI simulation that implements the random walkers approach. A comparison of the Monte-Carlo/random walkers approach with the FEM approach is beyond the scope of this paper. SpinDoctor offers an alternative, solving the same physics problem using PDEs.

After surveying other works on dMRI simulations, we saw a need to have a simulation toolbox that provides a way to easily define geometrical configurations. In SpinDoctor we have tried to offer useful configurations, without being overly general. Allowing too much generality in the geometrical configurations would have made code robustness very difficult to achieve due to the difficulties related to problems in computational geometry (high quality surface triangulation, robust FE mesh generation). The geometrical configuration routines provided by SpinDoctor are a helpful front end, to enable dMRI researchers to get started quickly to perform numerical simulations. Those users who already have a high quality surface triangulation can use the other parts of SpinDoctor without passing through this front end.

The bulk of SpinDoctor is the numerical solutions of two PDEs. When one is only interested in the ADC, then computing the H-ADC model is the good option. When one is interested in higher order behavior in the dMRI signal, then the BTPDE model is a good option for accessing high b-value behavior.

Because time stepping methods for semi-discretized linear systems arising from finite element discretization is a well-studied subject in the mathematical literature, the ODE solvers implemented in Matlab already optimize for such linear systems. For example, the mass matrix is passed into the ODE solver as an optional parameter so to avoid explicit matrix inversion. In addition, the ODE solution is guaranteed to stay within a user-requested residual tolerance. We believe this type of optimization and error control is clearly advantageous over simulation codes that do not have it.

To mimic the phenomenon where the water molecules can enter and exit the computational domain, the pseudo-periodic boundary conditions were implemented in [28–30]. At this stage, we have chosen not to implement this in SpinDoctor, instead, spins are not allowed to leave the computational domain. Implementing pseudo-periodic boundary conditions would make the code more complicated, and it remains to be seen if it is a desired features among potential users. If it is, then it could be part of a future development.

The twisting and bending of the canonical configuration is something unique to SpinDoctor. It

removes many computational geometry difficulties by meshing first the canonical configuration before deforming the FE mesh via an analytical coordinate transformation. This is a way to simulate fibers that are not parallel, that bend, for example. For fibers that disperse, perhaps more complicated analytical coordinate transformations can be performed on the canonical configuration to mimic that situation. This is a possible future direction to explore.

SpinDoctor depends on Matlab for the ODE solve routines as well as for the computational geometry routines to produce the tight wrap ECS. To implement SpinDoctor outside of Matlab would require replacing these two set of Matlab routines. Other routines of SpinDoctor can be easily implemented in another programming language.

SpinDoctor can be downloaded at <https://github.com/jingrebeccali/SpinDoctor>.

6. Conclusion

This paper describes a publicly available Matlab toolbox called SpinDoctor that can be used to solve the BTPDE to obtain the dMRI signal and to solve the DE of the H-ADC model to obtain the ADC. SpinDoctor is a software package that seeks to reduce the work required to perform numerical simulations for dMRI for prototyping purposes.

SpinDoctor provides built-in options of including spherical cells with a nucleus, cylindrical cells with a myelin layer, an extra-cellular space (ECS) enclosed either in a box or in a tight wrapping around the cells. The deformation of canonical cells by bending and twisting is implemented via an analytical coordinate transformation of the FE mesh. Permeable membranes for the BT-PDE is implemented using double nodes on the compartment interfaces. Built-in diffusion-encoding pulse sequences include the Pulsed Gradient Spin Echo and the Oscilating Gradient Spin Echo. Error control in the time stepping is done using built-in Matlab ODE solver routines.

User feedback to improve SpinDoctor is welcomed.

Acknowledgment

The authors gratefully acknowledge the *French-Vietnam Master in Applied Mathematics* program whose students (co-authors on this paper, Van-Dang Nguyen, Try Nguyen Tran, Bang Cong Trang, Khieu Van Nguyen, Vu Duc Thach Son, Hoang An Tran, Hoang Trong An Tran, Thi Minh Phuong Nguyen) have contributed to the SpinDoctor project during their internships in France in the past several years, as well as the *Vice-Presidency for Marketing and International Relations* at Ecole Polytechnique for financially supporting a part of the students' stay. Jan Valdman was supported by the Czech Science Foundation (GACR), through the grants GA18-03834S and GA17-04301S. Van-Dang Nguyen was supported by the Swedish Energy Agency, Sweden with the project ID P40435-1 and MSO4SC with the grant number 731063.

References

- [1] E. L. Hahn, Spin echoes, Phys. Rev. 80 (1950) 580–594.

- [2] E. O. Stejskal, J. E. Tanner, Spin diffusion measurements: Spin echoes in the presence of a time-dependent field gradient, *The Journal of Chemical Physics* 42 (1) (1965) 288–292. doi:10.1063/1.1695690.
- [3] D. L. Bihan, E. Breton, D. Lallemand, P. Grenier, E. Cabanis, M. Laval-Jeantet, MR imaging of intravoxel incoherent motions: application to diffusion and perfusion in neurologic disorders., *Radiology* 161 (2) (1986) 401–407, pMID: 3763909.
- [4] M. D. Does, E. C. Parsons, J. C. Gore, Oscillating gradient measurements of water diffusion in normal and globally ischemic rat brain, *Magn. Reson. Med.* 49 (2) (2003) 206–215. doi:10.1002/mrm.10385.
- [5] J. H. Jensen, J. A. Helpert, A. Ramani, H. Lu, K. Kaczynski, Diffusional kurtosis imaging: The quantification of non-Gaussian water diffusion by means of magnetic resonance imaging, *Magnetic Resonance in Medicine* 53 (6) (2005) 1432–1440. doi:10.1002/mrm.20508.
- [6] D. S. Tuch, T. G. Reese, M. R. Wiegell, N. Makris, J. W. Belliveau, V. J. Wedeen, High angular resolution diffusion imaging reveals intravoxel white matter fiber heterogeneity, *Magnetic Resonance in Medicine* 48 (4) (2002) 577–582. arXiv:<https://onlinelibrary.wiley.com/doi/pdf/10.1002/mrm.10268>, doi:10.1002/mrm.10268. URL <https://onlinelibrary.wiley.com/doi/abs/10.1002/mrm.10268>
- [7] Y. Assaf, T. Blumenfeld-Katzir, Y. Yovel, P. J. Basser, Axc caliber: A method for measuring axon diameter distribution from diffusion MRI, *Magn. Reson. Med.* 59 (6) (2008) 1347–1354. URL <http://dx.doi.org/10.1002/mrm.21577>
- [8] D. C. Alexander, P. L. Hubbard, M. G. Hall, E. A. Moore, M. Ptito, G. J. Parker, T. B. Dyrby, Orientationally invariant indices of axon diameter and density from diffusion mri, *NeuroImage* 52 (4) (2010) 1374–1389. URL <http://www.sciencedirect.com/science/article/pii/S1053811910007755>
- [9] H. Zhang, P. L. Hubbard, G. J. Parker, D. C. Alexander, Axon diameter mapping in the presence of orientation dispersion with diffusion mri, *NeuroImage* 56 (3) (2011) 1301–1315. URL <http://www.sciencedirect.com/science/article/pii/S1053811911001376>
- [10] H. Zhang, T. Schneider, C. A. Wheeler-Kingshott, D. C. Alexander, Noddi: Practical in vivo neurite orientation dispersion and density imaging of the human brain, *NeuroImage* 61 (4) (2012) 1000–1016. URL <http://www.sciencedirect.com/science/article/pii/S1053811912003539>
- [11] L. M. Burcaw, E. Fieremans, D. S. Novikov, Mesoscopic structure of neuronal tracts from time-dependent diffusion, *NeuroImage* 114 (2015) 18 – 37. doi:10.1016/j.neuroimage.2015.03.061.
- [12] M. Palombo, C. Ligneul, J. Valette, Modeling diffusion of intracellular metabolites in the mouse brain up to very high diffusion-weighting: Diffusion in long fibers (almost) accounts for non-monoexponential attenuation, *Magnetic Resonance in Medicine* 77 (1) (2017) 343–350. doi:10.1002/mrm.26548.

- [13] M. Palombo, C. Ligneul, C. Najac, J. Le Douce, J. Flament, C. Escartin, P. Hantraye, E. Brouillet, G. Bonvento, J. Valette, New paradigm to assess brain cell morphology by diffusion-weighted MR spectroscopy in vivo, *Proceedings of the National Academy of Sciences* 113 (24) (2016) 6671–6676. arXiv:<http://www.pnas.org/content/113/24/6671.full.pdf>, doi:10.1073/pnas.1504327113.
- [14] L. Ning, E. Özarslan, C.-F. Westin, Y. Rathi, Precise inference and characterization of structural organization (picaso) of tissue from molecular diffusion, *NeuroImage* 146 (2017) 452 – 473. doi:10.1016/j.neuroimage.2016.09.057.
- [15] E. Fieremans, J. H. Jensen, J. A. Helpert, White matter characterization with diffusional kurtosis imaging, *NeuroImage* 58 (1) (2011) 177 – 188.
- [16] E. Panagiotaki, T. Schneider, B. Siow, M. G. Hall, M. F. Lythgoe, D. C. Alexander, Compartment models of the diffusion mr signal in brain white matter: A taxonomy and comparison, *NeuroImage* 59 (3) (2012) 2241–2254.
URL <http://www.sciencedirect.com/science/article/pii/S1053811911011566>
- [17] S. N. Jespersen, C. D. Kroenke, L. Astergaard, J. J. Ackerman, D. A. Yablonskiy, Modeling dendrite density from magnetic resonance diffusion measurements, *NeuroImage* 34 (4) (2007) 1473–1486.
URL <http://www.sciencedirect.com/science/article/pii/S1053811906010950>
- [18] A. Ianuş, D. C. Alexander, I. Drobnjak, Microstructure imaging sequence simulation toolbox, in: S. A. Tsaftaris, A. Gooya, A. F. Frangi, J. L. Prince (Eds.), *Simulation and Synthesis in Medical Imaging*, Springer International Publishing, Cham, 2016, pp. 34–44.
- [19] I. Drobnjak, H. Zhang, M. G. Hall, D. C. Alexander, The matrix formalism for generalised gradients with time-varying orientation in diffusion nmr, *Journal of Magnetic Resonance* 210 (1) (2011) 151 – 157. doi:10.1016/j.jmr.2011.02.022.
URL <http://www.sciencedirect.com/science/article/pii/S1090780711000838>
- [20] B. D. Hughes, *Random walks and random environments* / Barry D. Hughes, Clarendon Press Oxford ; New York, 1995.
- [21] C.-H. Yeh, B. Schmitt, D. Le Bihan, J.-R. Li-Schlittgen, C.-P. Lin, C. Poupon, Diffusion microscopist simulator: A general monte carlo simulation system for diffusion magnetic resonance imaging, *PLoS ONE* 8 (10) (2013) e76626. doi:10.1371/journal.pone.0076626.
- [22] M. Hall, D. Alexander, Convergence and parameter choice for monte-carlo simulations of diffusion mri, *Medical Imaging, IEEE Transactions on* 28 (9) (2009) 1354 –1364. doi: 10.1109/TMI.2009.2015756.
- [23] G. T. Balls, L. R. Frank, A simulation environment for diffusion weighted mr experiments in complex media, *Magn. Reson. Med.* 62 (3) (2009) 771–778.
URL <http://dx.doi.org/10.1002/mrm.22033>
- [24] K. V. Nguyen, E. H. Garzon, J. Valette, Efficient gpu-based monte-carlo simulation of diffusion in real astrocytes reconstructed from confocal microscopy, *Journal of Magnetic Resonance* doi: 10.1016/j.jmr.2018.09.013.
URL <http://www.sciencedirect.com/science/article/pii/S1090780718302386>

- [25] H. Hagslatt, B. Jonsson, M. Nyden, O. Soderman, Predictions of pulsed field gradient NMR echo-decays for molecules diffusing in various restrictive geometries. simulations of diffusion propagators based on a finite element method, *Journal of Magnetic Resonance* 161 (2) (2003) 138–147.
URL <http://www.sciencedirect.com/science/article/pii/S1090780702000393>
- [26] N. Loren, H. Hagslatt, M. Nyden, A.-M. Hermansson, Water mobility in heterogeneous emulsions determined by a new combination of confocal laser scanning microscopy, image analysis, nuclear magnetic resonance diffusometry, and finite element method simulation, *The Journal of Chemical Physics* 122 (2) (2005) –. doi:10.1063/1.1830432.
- [27] B. F. Moroney, T. Stait-Gardner, B. Ghadirian, N. N. Yadav, W. S. Price, Numerical analysis of NMR diffusion measurements in the short gradient pulse limit, *Journal of Magnetic Resonance* 234 (0) (2013) 165–175.
URL <http://www.sciencedirect.com/science/article/pii/S1090780713001572>
- [28] J. Xu, M. Does, J. Gore, Numerical study of water diffusion in biological tissues using an improved finite difference method, *Physics in medicine and biology* 52 (7).
URL <http://view.ncbi.nlm.nih.gov/pubmed/17374905>
- [29] J.-R. Li, D. Calhoun, C. Poupon, D. L. Bihan, Numerical simulation of diffusion mri signals using an adaptive time-stepping method, *Physics in Medicine and Biology* 59 (2) (2014) 441.
URL <http://stacks.iop.org/0031-9155/59/i=2/a=441>
- [30] D. V. Nguyen, J.-R. Li, D. Grebenkov, D. Le Bihan, A finite elements method to solve the Bloch-Torrey equation applied to diffusion magnetic resonance imaging, *Journal of Computational Physics* 263 (0) (2014) 283–302.
URL <http://www.sciencedirect.com/science/article/pii/S0021999114000308>
- [31] L. Beltrachini, Z. A. Taylor, A. F. Frangi, A parametric finite element solution of the generalised bloch-torrey equation for arbitrary domains, *Journal of Magnetic Resonance* 259 (2015) 126 – 134. doi:<https://doi.org/10.1016/j.jmr.2015.08.008>.
URL <http://www.sciencedirect.com/science/article/pii/S1090780715001743>
- [32] G. Russell, K. D. Harkins, T. W. Secomb, J.-P. Galons, T. P. Trouard, A finite difference method with periodic boundary conditions for simulations of diffusion-weighted magnetic resonance experiments in tissue, *Physics in Medicine and Biology* 57 (4) (2012) N35.
URL <http://stacks.iop.org/0031-9155/57/i=4/a=N35>
- [33] J. G. Verwer, W. H. Hundsdorfer, B. P. Sommeijer, Convergence properties of the Runge-Kutta-Chebyshev method, *Numerische Mathematik* 57 (1990) 157–178. doi:10.1007/BF01386405.
- [34] V. D. Nguyen, A FEniCS-HPC framework for multi-compartment Bloch-Torrey models, Vol. 1, 2016, pp. 105–119, QC 20170509.
URL <https://www.eccomas2016.org/>
- [35] V.-D. Nguyen, J. Jansson, J. Hoffman, J.-R. Li, A partition of unity finite element method for computational diffusion mri, *Journal of Computational Physics* doi:10.1016/j.jcp.2018.08.039.
URL <http://www.sciencedirect.com/science/article/pii/S0021999118305709>

- [36] V.-D. Nguyen, J. Jansson, H. T. A. Tran, J. Hoffman, J.-R. Li, Diffusion mri simulation in thin-layer and thin-tube media using a discretization on manifolds, *Journal of Magnetic Resonance* 299 (2019) 176 – 187. doi:<https://doi.org/10.1016/j.jmr.2019.01.002>.
URL <http://www.sciencedirect.com/science/article/pii/S1090780719300023>
- [37] H. Si, Tetgen, a delaunay-based quality tetrahedral mesh generator, *ACM Trans. Math. Softw.* 41 (2) (2015) 11:1–11:36. doi:[10.1145/2629697](https://doi.org/10.1145/2629697).
URL <http://doi.acm.org/10.1145/2629697>
- [38] T. Rahman, J. Valdman, Fast matlab assembly of fem matrices in 2d and 3d: nodal elements, *Applied Mathematics and Computation* (219) (2013) 7151–7158.
- [39] D. V. Nguyen, J.-R. Li, D. Grebenkov, D. L. Bihan, A finite elements method to solve the bloch–torrey equation applied to diffusion magnetic resonance imaging, *Journal of Computational Physics* 263 (0) (2014) 283 – 302. doi:[10.1016/j.jcp.2014.01.009](https://doi.org/10.1016/j.jcp.2014.01.009).
URL <http://www.sciencedirect.com/science/article/pii/S0021999114000308>
- [40] P. T. Callaghan, J. Stepianik, Frequency-domain analysis of spin motion using modulated-gradient NMR, *Journal of Magnetic Resonance, Series A* 117 (1) (1995) 118–122.
URL <http://www.sciencedirect.com/science/article/pii/S1064185885799597>
- [41] S. Schiavi, H. Haddar, J.-R. Li, A macroscopic model for the diffusion mri signal accounting for time-dependent diffusivity, *SIAM Journal on Applied Mathematics* Accepted.
- [42] P. P. Mitra, P. N. Sen, L. M. Schwartz, P. Le Doussal, Diffusion propagator as a probe of the structure of porous media, *Physical review letters* 68 (24) (1992) 3555–3558.
- [43] P. P. Mitra, P. N. Sen, L. M. Schwartz, Short-time behavior of the diffusion coefficient as a geometrical probe of porous media, *Phys. Rev. B* 47 (1993) 8565–8574.
- [44] D. S. Grebenkov, Pulsed-gradient spin-echo monitoring of restricted diffusion in multilayered structures, *Journal of Magnetic Resonance* 205 (2) (2010) 181–195.
URL <http://www.sciencedirect.com/science/article/pii/S1090780710001199>

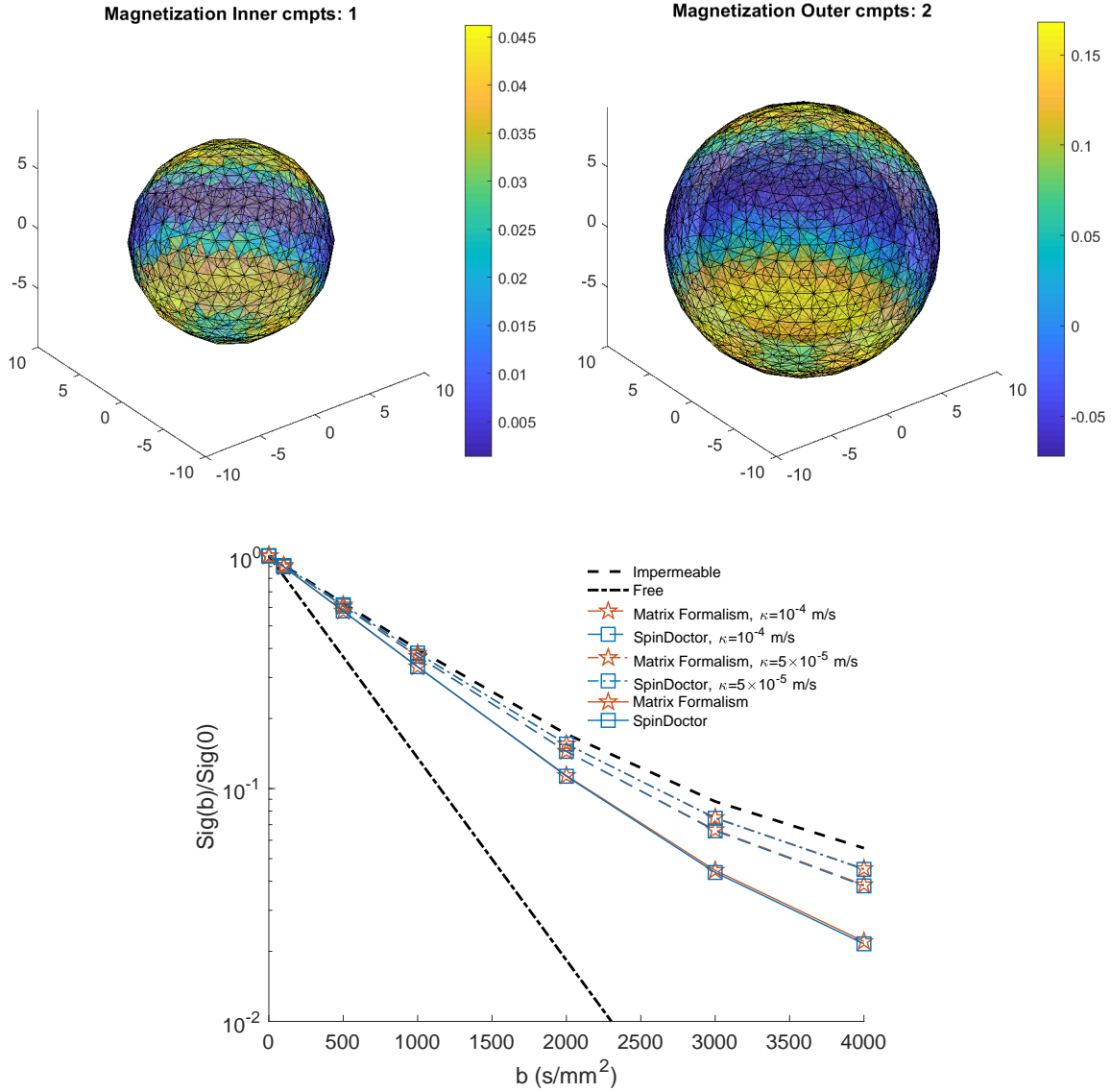


Figure 5: Top: Solution for $\kappa = 5 \times 10^{-5}$ m/s, $\sigma^{in} = \sigma^{out} = 2 \times 10^{-3}$ mm^2/s , no ECS, PGSE ($\delta = 2.5\text{ms}$, $\Delta = 10\text{ms}$); Bottom: $R_1 = \frac{4}{3}R_2 = 10\mu\text{m}$, $\kappa = [10^{-3}, 10^{-4}, 5 \times 10^{-5}]$ m/s, $\text{H}_{tetgen}=1.0$ ($h_{max} = 1.5$), maximum relative errors 2.26%, 1.06%, and 0.68%.

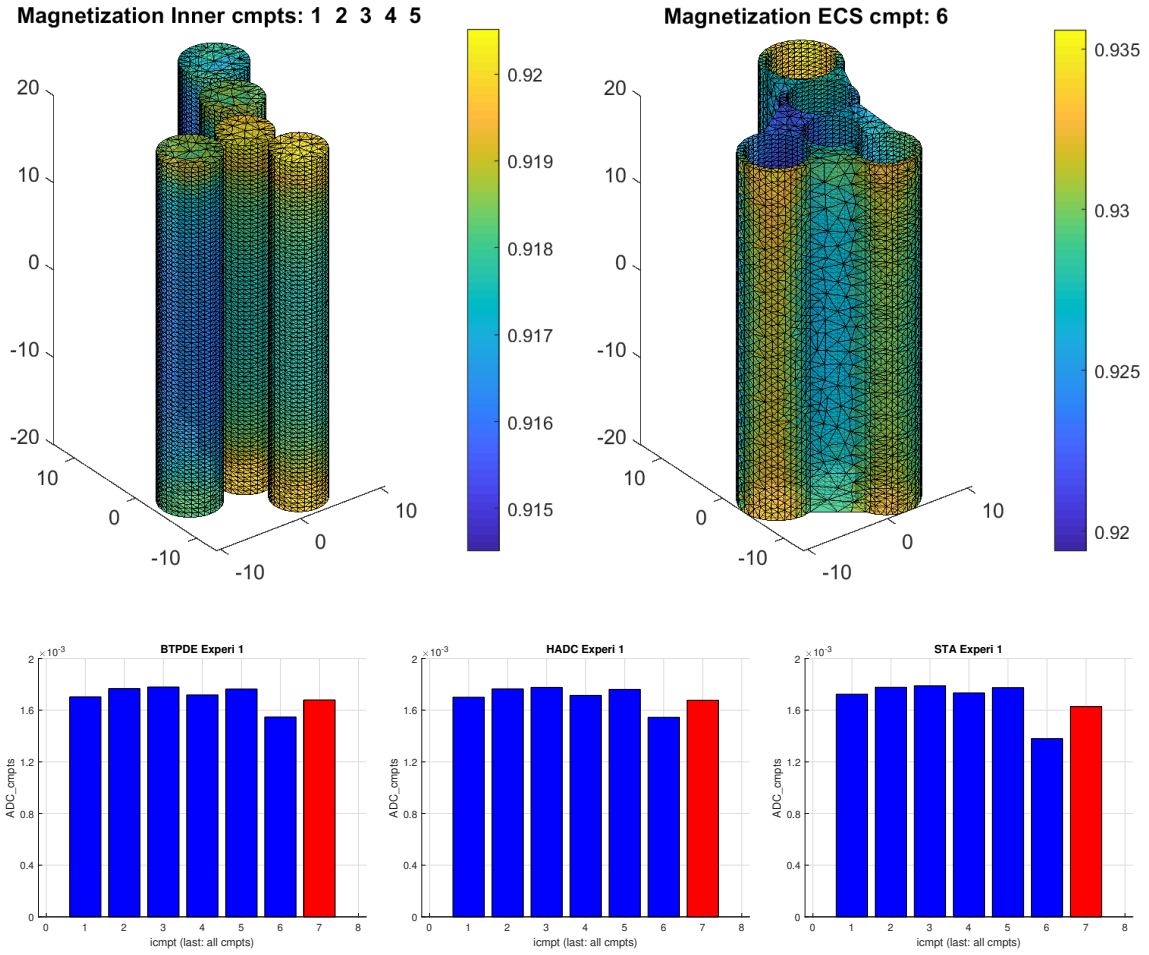


Figure 6: Geometry: 5 cylinders, tight wrap ECS, ECS gap = 0.2, $\mathbf{u}_g = [1, 1, 1]$, $\sigma^{out} = \sigma^{ecs} = 2 \times 10^{-3} \text{ mm}^2/\text{s}$, $\kappa = 0 \text{ m/s}$, OGSE cosine ($\delta = 14 \text{ ms}$, $\Delta = 14 \text{ ms}$, number of periods = 6). The vertical bars indicate the ADC in each compartment. The ADC in the rightmost position is the ADC that takes into account the diffusion in all the compartments.

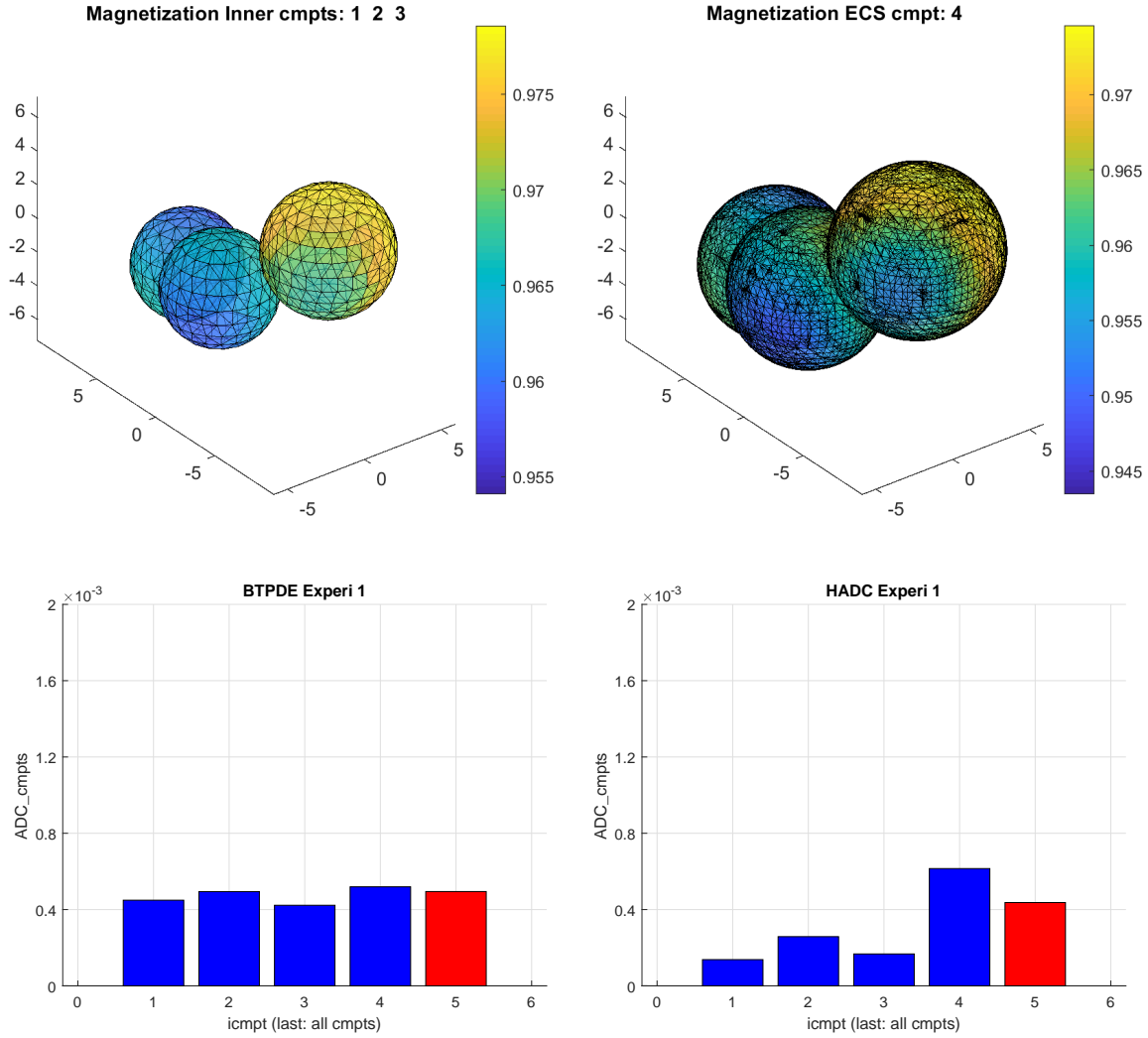


Figure 7: Geometry: 3 spheres, tight wrap ECS, ECS gap = 0.3, $\mathbf{u}_g = [1, 1, 0]$, $\sigma^{in} = \sigma^{ecs} = 2 \times 10^{-3} \text{ mm}^2/\text{s}$, $\kappa = 1 \times 10^{-3} \text{ m/s}$ (left), $\kappa = 0 \text{ m/s}$ (right). PGSE ($\delta = 5\text{ms}, \Delta = 5\text{ms}$). The vertical bars indicate the ADC in each compartment. The ADC in the rightmost position is the ADC that takes into account the diffusion in all the compartments.

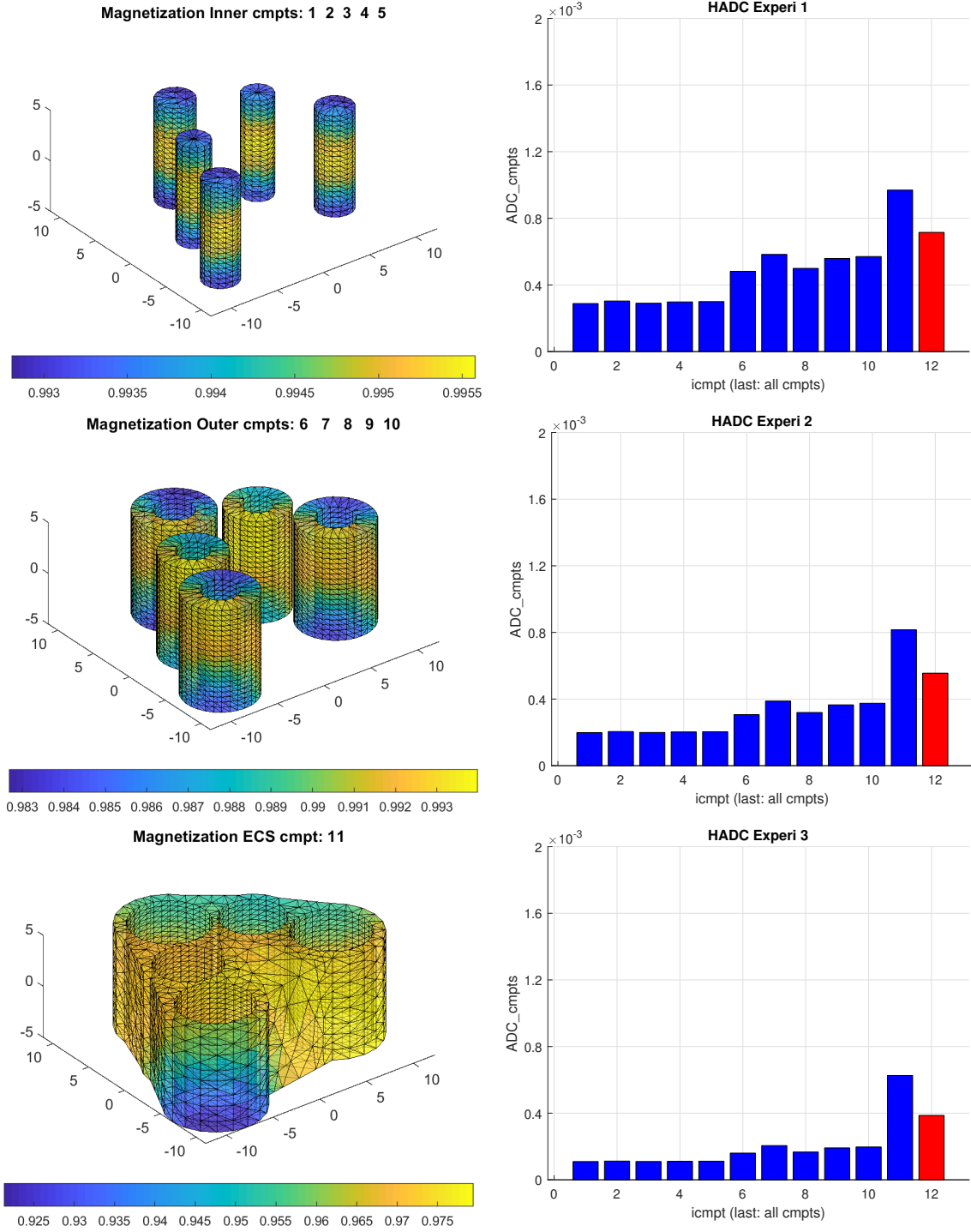


Figure 8: Geometry: 5 cylinders, myelin layer, $R_{in}/R_{out} = 0.5$, tight wrap ECS, ECS gap = 0.3, $\kappa = 0$ m/s, $\mathbf{u}_g = [1, 1, 1]$, $\sigma^{in} = \sigma^{out} = \sigma^{ecs} = 2 \times 10^{-3}$ mm²/s, 3 experiments: PGSE ($\delta = 5$ ms, $\Delta = 5, 10, 20$ ms). The vertical bars indicate the ADC in each compartment. The ADC in the rightmost position is the ADC that takes into account the diffusion in all the compartments.

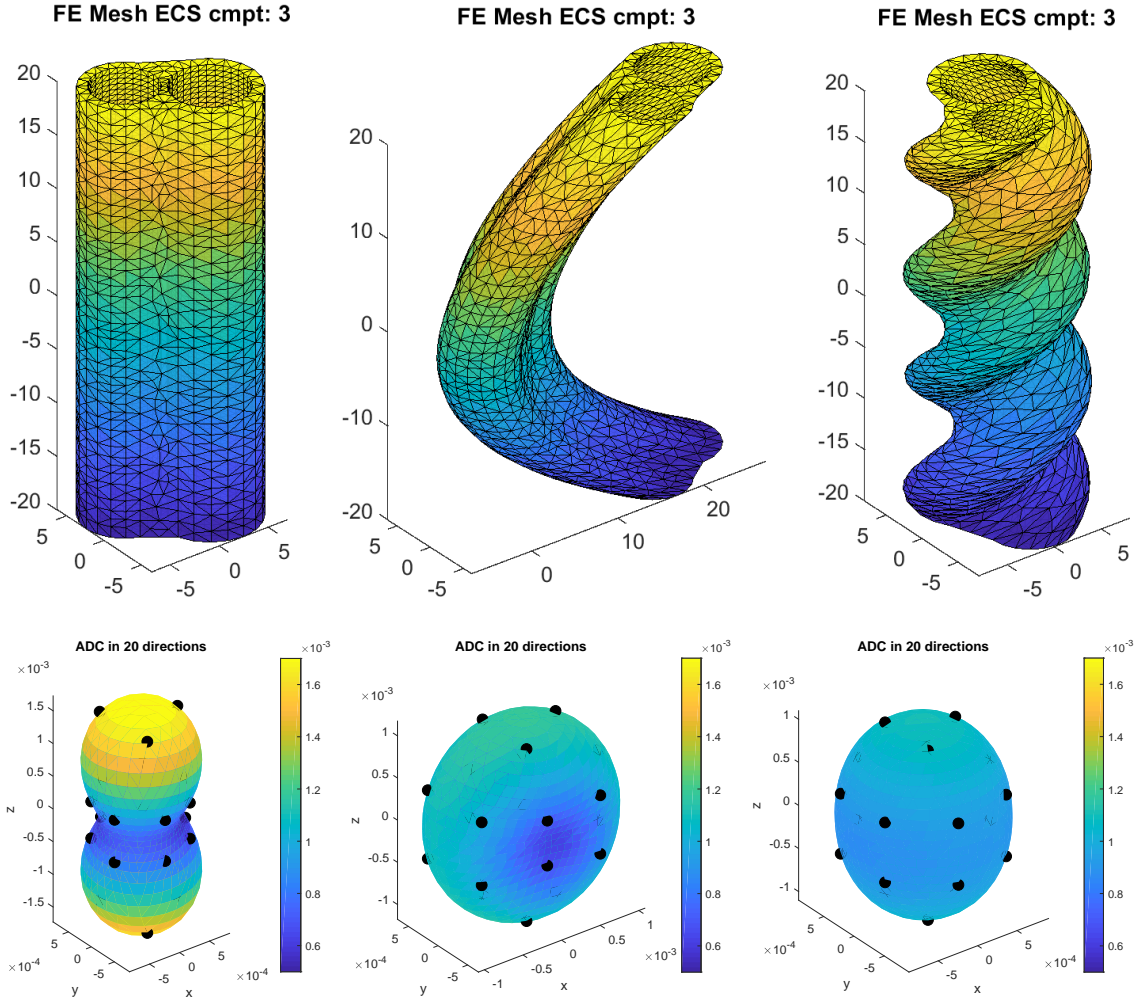


Figure 9: Geometry: 2 cylinders, no myelin layer, tight wrap ECS, ECS gap = 0.3, $\kappa = 0$ m/s, $\sigma^{out} = \sigma^{ecs} = 2 \times 10^{-3}$ mm²/s, PGSE ($\delta = 2.5$ ms, $\Delta = 5$ ms).

Left: canonical configuration. Middle: bend parameter = 0.05. Right: twist parameter = 0.30. Top: FE mesh of the ECS (the FE mesh of the axon compartments numbered 1 and 2 not shown). Bottom: interpolated values of the HADC on the unit sphere, and then the sphere was distorted to reflect the value of the HADC. The color axis also gives the value of the HADC in the various gradient directions. The black dots indicate the 20 original gradient-directions in which the HADC was simulated. The spherical harmonics interpolation takes to 20 original directions into 900 directions uniformly distributed on the sphere.